FFV-MBC: A Novel Fused Finger-Vein Recognition Method Based on Monogenic Binary Coding

Zhi-Yong Tao[1*], Meng Wang[1], Xin-Ru Zhou[1], Jie Li[2], Sen Lin[3]

[1] School of Electronics and Information Engineering, Liaoning Technical University, Huludao 125105, China
taozhiyong@lntu.edu.cn {wmegan, zxrxxn}@163.com
[2] Chinese Academy of Sciences Fujian Institute of Research on the Structure of Matter, Fuzhou 350002, China
leej95@163.com
[3] School of Automation and Electrical Engineering, Shenyang Ligong University, Shenyang 110159, China
lin_sen6@126.com

Abstract. To improve pattern representation capabilities and robustness in traditional finger-vein recognition algorithms. In this paper, we propose FFV-MBC, a novel fused finger-vein recognition method based on monogenic binary coding (MBC). First of all, the amplitude, orientation, and phase information of the finger-vein images are filtered by a multi-scale monogenic log-Gabor filter and encoded by the binary coding theory. Three local features, MBC-A, MBC-P, and MBC-O, are achieved from different combinations of local image intensity and variation coding. After obtaining the features, we utilize the block-based Fisher Linear Discriminant method to reduce the dimension. Finally, the similarity components are calculated by the cosine distance and fused for the final finger-vein recognition results. We evaluate our proposed method on two publicly available datasets and one self-built dataset, i.e., Malaysian Polytechnic University (FV-USM), the Group of Machine Learning and Applications of Shandong University (SDUMLA-HMT), and our team, Signal and Information Processing Laboratory (FV-SIPL). On average, the proposed method achieved high recognition accuracy, i.e., 99.30%, and 1.10% equal error rates (EER). Overall, the proposed method performs better than most classical and state-of-the-art finger-vein recognition methods.

Keywords: finger-vein recognition, monogenic binary coding, multi-scale monogenic log-Gabor filter, weighted fused

1 Introduction

Finger-vein recognition causes much interest in the researchers, with the contribution to information security and protection. As an essential way of biometric identification, it plays an irreplaceable role in personal data security.

Compared with other biometric features, such as fingerprint [1], palm print [2], face [3], iris [4], etc., finger-vein recognition has been widely applied for different scenarios due to high security, non-contact acquisition, difficult to copy, stability, and living recognition.

Generally speaking, finger-vein recognition includes four steps: finger-vein acquisition, image preprocessing, feature extraction, and matching, among which feature extraction is the most critical. More importantly, various feature extraction methodologies are utilized for finger-vein recognition, such as patterns, details, textures, and learnable features [5]. For example, vein pattern features were extracted through the average curvature method in [6]. The average curvature values of different directions for each point are used. Wang et al. [7] applied the scale-invariant feature transformation (SIFT) algorithm to extract detailed finger-vein features. The intersection point of finger-vein textures is chosen. After screening, the feature points available for matching and classification may be insufficient, thus increasing the probability of mismatching. Lu et al. [8] proposed a finger-vein recognition method combining the Gabor filter with the histogram of oriented gradients (HOG). However, the Gabor filters may increase the feature magnitude and cost much run-time. Wu et al. [9] designed a finger-vein recognition network combined with principal component analysis (PCA) [10] and linear discriminant analysis (LDA) [11]. After obtaining the region of interest (RoI) data, PCA and LDA are used to reduce the dimension of relevant feature vectors. PCA and LDA can obtain a spatial matrix converted from two-dimension to one-dimension. With the increasing number of image pixels, we might require large dimension computation and long run-time. Hence, its application scope has certain limitations. Also, the global methods are susceptible to changes in finger poses

---

* Corresponding Author

and lighting environments. Zhao et al. [12] used the complete local binary pattern (CLBP) and the statistical local binary pattern (SLBP) to describe the texture features of local veins. The local binary pattern (LBP) is used to describe images from pixel differences, resulting in good robust-ness to brightness and contrast changes. However, such methods focus on the relations between the center pixel and surroundings, while ignoring the information obtained from the center pixel itself.

In order to solve the above problems, we propose a novel fused finger-vein recognition method based on monogenic binary coding (MBC). First, inspired by the rotation-invariant monogenic signal in the MBC algorithm, we detect the monogenic amplitude, orientation, and phase information of the finger-vein images with orthogonal decomposition. Then, different features are generated from various combinations of local image intensity and variation coding. The feature dimension is reduced by the block-based Fisher Linear Discriminant (BFLD) [13]. Finally, we calculate the similarities of the two images by cosine distance and combine those of the three components at the score level. Experimental results show that FFV-MBC improves the accuracy and robustness of finger-vein recognition effectively. The main contributions of this paper are summarized as follows:

(1) Monogenic binary coding is used to effectively extract local features of the finger vein. Except for the relations between the center pixel and surroundings, the information obtained from the center pixel itself is used. The additional feature information effectively alleviates the influence of uneven illumination and low contrast on finger vein recognition.

(2) The finger-vein feature extracted by MBC is in high dimension and includes a lot of redundant information. This paper introduces the BFLD module to improve feature discrimination and reduce the dimension of the feature matrix.

(3) By fusing the feature similarities of different components of the monogenic signal, the discriminant feature can simultaneously proceed with energy, local structure, and geometric information. It enhances the feature representations and the recognition accuracies.

(4) A low-cost and portable finger-vein acquisition device is designed. A finger-vein dataset with good contrast and clear finger regions without excessive background information is produced. More clear and reliable finger-vein pictures are provided for subsequent recognition.

The remainder of this paper is presented as follows. Section 2 reviews some of the classic and state-of-the-art methods for finger-vein recognition. Section 3 introduces the principle of monogenic binary coding and the details of our proposed method. The parameter settings, accuracy, equal error rates (EER), run-times, etc., will be reported and analyzed in Section 4. Section 5 concludes the proposed method and the limitations.

2   Related Works

The existing finger-vein feature extraction methods can be roughly divided into machine learning-based, vein texture-based, and local feature-based methods. Machine learning-based methods include subspace learning and convolutional neural network learning. The subspace learning method can reduce some complex pre-processing steps and feature dimensions. Typically, Wang et al. [14] combined 2DPCA and 2DFLD (Fisher Linear Discriminant) techniques to improve recognition performance and reduce storage space. However, this method only extracts global features from the global perspective and lacks robustness to local intra-class changes, i.e., uneven illumination and rotation. The convolutional neural network can extract deeper features with strong generalization and representation ability. Zeng et al. [15] combined recurrent neural network, conditional random field, and residual network to extract vein texture features. The additional residual information improves the recognition performance of the system. However, this method needs to conduct a lot of training on the model after obtaining image features. It might get overfitting when constructing the complex model.

Classical methods are often based on vein texture, including curvature [16], repeated line tracking (RLT) [17], and morphological operation combined with the Gabor method [18]. Vasilopoulos et al. [19] exploited the enhanced maximum curvature method to extract vein pattern information and combine it with two matching methods to achieve good recognition performance on three public datasets. Nevertheless, this method relies on image segmentation technology, so it has high requirements for images. Zhang et al. [20] combined a Gabor filter with an improved histogram of oriented gradients to extract texture and orientation information from vein images. Although the Gabor filter is powerful in image texture analysis, it might lose essential information in low-quality vein images.

Some methods focus on local features for finger-vein recognition, i.e., local binary pattern [21], local line binary pattern (LLBP) [22], etc. Recently, Mustafa et al. [23] proposed a new finger-vein recognition system using a combination of complete local binary pattern and phase-only correlation. Compared with the classical local

feature extraction, this method can extract more detailed features. Zhao et al. [24] combined the mean and standard deviation of local region pixels by local binary pattern coding. This method makes up for the problem of insufficient global information extraction by classical local binary operators. Although these two methods have improved the local binary method, neither of them takes into account the information of the center pixel itself.

Most of the above research methods are aimed at identifying the single feature information in the image, more likely lacking some essential ones. Therefore, this paper proposes a novel fused finger-vein recognition method based on monogenic binary coding. The amplitude, phase, and direction information of the finger-vein image are extracted by the monogenic signal representation method, which is encoded by monogenic binary coding. The encoded features are then dimensionally reduced using BFLD to remove redundant information and reduce space complexity. Finally, the three features are fused in the matching stage, which effectively improves the performance of finger-vein recognition.

3 Proposed Method

3.1 Monogenic Signal Representations

As a two-dimensional extension of the one-dimensional analytical signal retaining the critical attributes, the monogenic signal [25] has been widely applied in the fields of image denoising, validation, and texture classification. The monogenic signal is generated from the Riesz transform, a multi-dimensional extension of the Hilbert transform [26]. In two-dimensional space, the Riesz transform is defined as:

$$f_R(z) = \begin{pmatrix} f_x(z) \\ f_y(z) \end{pmatrix} = \begin{pmatrix} h_x * f(z) \\ h_y * f(z) \end{pmatrix}, \; z = (x,y) \; . \tag{1}$$

The filters h_x and h_y are represented by two-dimensional frequency responses $-j\omega_x/\|\omega\|$ and $-j\omega_y/\|\omega\|$, in which ω denotes the angular frequency, $\omega = (\omega_x, \omega_y)$, $*$ means the convolution operation, and $f(z)$ refers to the input signal. The Riesz kernel in the spatial domain is defined as:

$$(h_x, h_y) = \left(\frac{x}{2\pi\|z\|^3}, \frac{y}{2\pi\|z\|^3} \right) \; . \tag{2}$$

In practice, the image needs to be band-pass filtered before inputting to the Riesz transform. The classical Gabor filter [27] is affected by bandwidth limitation and the direct current component. However, the logarithmic Gaussian function can make up for the deficiency of the Gabor function and represent the frequency responses more naturally. As a band-pass filter in our work, the frequency response of the Log-Gabor filter [28]:

$$G(\omega) = \exp\left\{ -\left[\log(\omega/\omega_0) \right]^2 \Big/ 2\left[\log(\sigma/\omega_0) \right]^2 \right\} \; , \tag{3}$$

$$\sigma = \sigma_{ratio}\omega_0, \; \omega_0 = \left(\lambda_{\min}\mu^{S-1} \right)^{-1} \; , \tag{4}$$

where ω_0 and σ are the center frequency and the scale variable, respectively. We utilize $\lambda_{\min}$ and μ to represent the minimum wavelength and the wavelength multiple. S and σ_{ratio} denote the number of scales and the scale factor. For the input image $f(z)$, the monogenic band-pass signal is represented by the combination of f and its Riesz transform:

$$\begin{cases} f_{\lg\_m}(z) = \left(f_{\lg}, f_{\lg\_x}, f_{\lg\_y} \right) \\ f_{\lg} = f(z) * F^{-1}\left(G(\omega) \right) \\ f_{\lg\_x} = h_x * f_{\lg} \\ f_{\lg\_y} = h_y * f_{\lg} \end{cases}, \tag{5}$$

where F^{-1} denotes the two-dimensional inverse Fourier transform. The original image signal is orthogonally decomposed into three components: local amplitude (A), local phase (P), and local orientation (O), as follows:

$$\begin{cases} A = \sqrt{ f_{\lg}^{\,2} + f_{\lg\_x}^2 + f_{\lg\_y}^2 } \\ P = -sign\left(f_{\lg\_x} \right) \text{atan2}\left(\sqrt{ f_{\lg\_x}^2 + f_{\lg\_y}^2 } \Big/ f_{\lg} \right) \,. \\ O = \text{atan}\left(f_{\lg\_y} / f_{\lg\_x} \right) \end{cases} \tag{6}$$

The local amplitude, phase, and orientation describe the local energy distribution, structure, and geometry information, respectively.

3.2 Monogenic Binary Coding

The monogenic signal is encoded in two steps, i.e., binary encoding methods with local variation and intensity [29]. Local variation binary coding focuses on the variation between the central and the surrounding pixels.

Due to different local properties of amplitude A, phase P, and orientation O, the local variation binary coding is separated into local amplitude and monogenic phase binary coding. The classical local variation coding process, a part of our work, is shown in the lower part of Fig. 1.
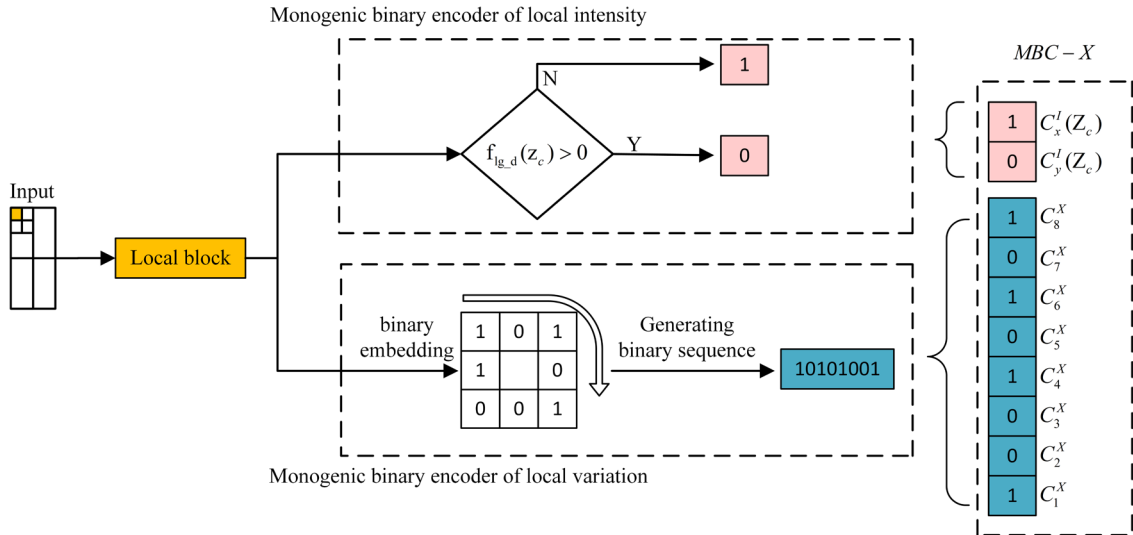

Fig. 1. The monogenic binary coding process of each local block (e.g., 3×3)
(The upper part is the monogenic local intensity encoder, and the lower is that of variation. These two coding methods are used to build $MBC - X$, where $X \in \{A, O, P\}$)

Similar to LBP, the local amplitude binary coding is encoded by comparing the amplitude values of the central and surrounding pixels. z_c and $A(z_c)$ denote the central pixel and its amplitude value. $A(i)$ indicates the amplitude value of the ith neighbor. The amplitude binary code of the ith neighbor is:

$$C_i^A(z_c) = \begin{cases} 1 & A(i) \geq A(z_c) \\ 0 & otherwise \end{cases} . \tag{7}$$

The angles of the local phase and orientation in the monogenic phase show the local structure and geometry information. Since feature type comparison works better than simple angles, we employ the quantization function $Q(x)$ to evaluate the similarity of two local features. They are considered similar only if the quantization function values of the two phases or orientations are equivalent. The phase and orientation binary coding rules for the ith neighbor are shown in Equation (8).

$$\begin{aligned} C_i^P(z_c) &= \begin{cases} 0 & Q(P(z_c)) = Q(P(i)) \\ 1 & otherwise \end{cases} \\ C_i^O(z_c) &= \begin{cases} 0 & Q(O(z_c)) = Q(O(i)) \\ 1 & otherwise \end{cases} \end{aligned}, \tag{8}$$

where, $Q(x) = q$, $\frac{360 \cdot (q-1)}{4} \leq x \leq \frac{360 \cdot q}{4}$, $P(i)$ and $O(i)$ indicate the local phase and orientation of the ith pixel in the neighborhood around the central pixel. Therefore, the overall binary code of local variation of the monogenic signal is defined:

$$C_A(z_c) = \left[C_N^A, C_{N-1}^A, \cdots, C_1^A \right]_{binary} . \tag{9}$$

$$C_P(z_c) = \left[C_N^P, C_{N-1}^P, \cdots, C_1^P \right]_{binary} . \tag{10}$$

$$C_O(z_c) = \left[C_N^O, C_{N-1}^O, \cdots, C_1^O \right]_{binary} . \tag{11}$$

The local intensity coding adopts the quadrant-bit method to encode the local intensity feature information of the central pixel, in the upper part of Fig. 1, where $f_{lg\_d}, d \in \{x, y\}$, represent the horizontal and vertical Riesz transform outputs of the monogenic signal representation. The encoding form of quadrant-bit methods is: $[C_x^I(z_c), C_y^I(z_c)]_{binary}$, regarded as the highest two bits in MBC code.

$$C_d^I(z_c) = \begin{cases} 0 & f_{lg\_d}(z_c) > 0 \\ 1 & f_{lg\_d}(z_c) \leq 0 \end{cases}, d \in \{x, y\} . \tag{12}$$

MBC-A, MBC-P, and MBC-O represent different binary coding methods of the three components of the monogenic signal. To be specific, in each binary encoding method, the local intensity and variation codes are regarded as the two highest and the other eight low bits:

$$\begin{cases} MBC\text{-}A(z_c) = \left[C_x^I(z_c), C_y^I(z_c), C_A(z_c) \right]_{binary} \\ MBC\text{-}P(z_c) = \left[C_x^I(z_c), C_y^I(z_c), C_P(z_c) \right]_{binary} \\ MBC\text{-}O(z_c) = \left[C_x^I(z_c), C_y^I(z_c), C_O(z_c) \right]_{binary} \end{cases} . \tag{13}$$

3.3 Proposed Algorithm

Local histograms can represent local feature information, with the advantages of robustness to illumination

changes and background noise. After obtaining the multi-scale $MBC-X$ feature map of the finger-vein image, we construct the $MBC-X$ histogram. If feature histogram fusion is performed before their matching, the feature dimension and algorithm complexity will be increased. Therefore, we introduce the BFLD module to enhance the discrimination and reduce the feature dimension. Then feature points are matched by cosine distance, and similarity fusion is further carried out. The flowchart of the proposed methodology is demonstrated in Fig. 2. Considering the rationality and feasibility, the overall framework can be divided into five steps as follows.
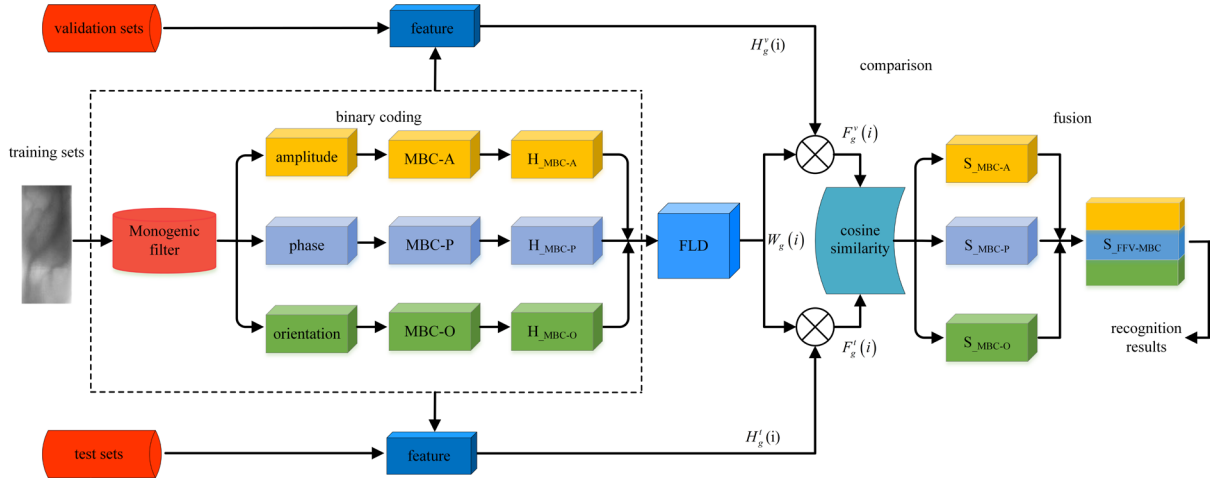

Fig. 2. The overall flowchart of our proposed method

(1) For the two-dimensional input $f(z)$, the monogenic signal is decomposed into the monogenic amplitude, orientation, and phase information through the Riesz transform and Log-Gabor filter. Corresponding to the monogenic binary coding mechanism, the three monogenic components are encoded to construct the feature maps.

(2) The encoded image is divided into M parent blocks, which are further split into K sub-blocks, where $M = M_a \times M_b$, $K = M_c \times M_d$. Next, we extract the histogram features of each sub-block and concatenate the local histograms of all different sub-blocks into a single vector to represent the histogram of the parent block.

(3) The parent block feature vectors H_K^L corresponding to all training sets are extracted by the second step to form M feature sets, $H_i = \left[H_K^1, H_K^2, H_K^3, \cdots, H_K^L \right]$, where $i = 1, 2, 3, \cdots, M$, with L training pictures. We reduce the dimension of feature vector $H_g(i)$ via PCA and obtain the best projection vector-matrix $W_g(i)$ through Fisher criterion, where $g \in \{MBC-A, MBC-O, MBC-P\}$.

(4) The validation and test sets are partitioned in the same proportion to achieve the feature sets $H_g^v(i)$ and $H_g^t(i)$. The features of each parent block are projected onto $W_g(i)$, resulting in low-dimensional vectors in Fisher space, $F_g^v(i)$ and $F_g^t(i)$, where $F_g(i) = [W_g(i)]^T H_g(i)$. Finally, the cosine distance is utilized to measure the similarities between the validation and test sets. We select $F_g^v(i)$ and $F_g^t(i)$ to represent the ith low-dimensional feature of the validation and test sets. The similarity between $F_g^v(i)$ and $F_g^t(i)$ is calculated as:

$$S_g(F_g^v(i), F_g^t(i)) = \frac{< F_g^v(i), F_g^t(i) >}{\left\| F_g^v(i) \right\| \left\| F_g^t(i) \right\|} \quad . \tag{14}$$

The similarities between the images of the entire validation and test sets are represented by the similarity accumulation of M parent blocks in Equation (15), the same for similarity calculation of amplitude S_{MBC-A}, phase S_{MBC-P}, and orientation S_{MBC-O}.

$$S_g(F_g^v, F_g^t) = \sum_{i=1}^{M} S_g(F_g^v(i), F_g^t(i)) \ . \tag{15}$$

(5) In order to obtain better recognition results, we combine features with the appropriate weights to gain $S_{FFV-MBC}$ and contribute to the final recognition task, where a_1, a_2, and a_3 represent coefficients, subject to $a_1 + a_2 + a_3 = 1$.

$$S_{FFV-MBC} = a_1 S_{MBC-P} + a_2 S_{MBC-A} + a_3 S_{MBC-O} \ . \tag{16}$$

Improper weight division might cause accuracy decline. Since the performances of local amplitude and local orientation are relatively close in various databases, we assign the same weight to S_{MBC-A} and S_{MBC-O}. Specific experimental results will be described in detail in the fourth chapter.

4 Experimental Results and Analysis

Our experiments are conducted on Windows 10 with Intel Core i7-5500U and 8GB memory. To verify the superiority of the FFV-MBC method proposed in this paper, we conduct a series of experiments on two public datasets and one self-built dataset. The proposed method is evaluated in terms of accuracy and EER. All the time in the experiment is the recognition run-time of a single image. The experimental details and the superiority of our proposed model are shown in this section. Note that the collection and essential technical details of the self-built dataset are also included.

4.1 Datasets

We created a new, high-quality finger-vein dataset in the Signal and Information Processing Laboratory (FV-SIPL). Except for the self-built dataset, we evaluate the proposed method on the datasets made by Malaysian Polytechnic University (FV-USM) [30], the Group of Machine Learning and Applications of Shandong University (SDUMLA-HMT) [31]. An overview of the three datasets is shown in Table 1. The third column, 'sample', shows the number of samples for each finger.

Table 1. Information about the finger-vein datasets used in our experiments

Dataset	# People	Details of fingers	Sample	# Images
FV-USM	123	Index, middle (both hands)	12	5904
SDUMLA-HMT	106	Index, middle, ring (both hands)	6	3816
FV-SIPL	27	Index, middle (both hands)	12	1296

FV-USM was collected from 123 people, each of whom provided two index and middle fingers and participated in two collection processes. Each finger's picture should be taken six times with the size of 640×480 pixels in each collection process. For SDUMLA-HMT, the Joint Laboratory made the acquisition equipment for the Intelligent Computing and Intelligent System of Shandong University. This dataset was obtained from 106 people, each of whom provided the index, middle, and ring fingers of both hands. Each finger was collected six times repeatedly with the size of 320×240 pixels.

The source of the self-built dataset includes 27 volunteers, of whom are teachers and students from Liaoning Technical University. Each volunteer provided four fingers, and each finger was collected 12 times, generating a total of 1296 ($27 \times 4 \times 12$) finger-vein pictures. The finger veins in our dataset (FV-SIPL) appear in 176×415 pixels with higher quality, fewer non-finger areas, and no apparent flipping of different images of the same finger.

Self-built Dataset. We collected the dataset FV-SIPL through a self-built finger-vein acquisition sensor with a single camera. Here are the collection details of the finger-vein images in FV-SIPL.

(1) Side-illuminated light penetration. The hemoglobin in the blood possesses a strong absorption capacity for near-infrared rays with a wavelength of $720 \sim 1104$ nanometers. When the incident light adopts this wavelength, the near-infrared light is absorbed by hemoglobin in the blood vessel and reflected by other finger tissues.

Therefore, the finger-vein structure can be highlighted in the imaging system [32].

Generally, the finger-vein image acquisition devices are divided into light penetration and reflection acquisition. Compared with the reflective acquisition, the infrared light of the light penetration acquisition is in a relatively closed environment. Because of inherent advantages, the light penetration collection results in higher-quality images. As shown in Fig. 3, the light penetration method can be further divided into top-illuminated and side-illuminated (left and right sides). If the illumination is not uneven, the contrast between the venous and non-vein areas may be greatly reduced. After angle adjustments, the finger-vein collection device built by our laboratory adopts the side-illuminated light penetration method finally, as shown in Fig. 3(b).
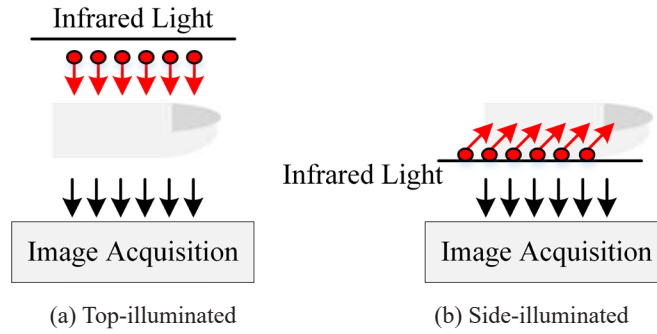

(a) Top-illuminated   (b) Side-illuminated

Fig. 3. Two types of light penetration in finger-vein acquisition

(2) Sensor selection. Besides, our device adopts 850 nm near-infrared led and embeds an infrared high transmittance filter (NIR filter) to eliminate the interference of noisy background and visible light. First, a 1080p resolution near-infrared camera is used to shoot images. Second, the LED light intensity is automatically adjusted by pulse width modulation (PWM) according to the image's brightness. Finally, the camera can catch a clearer image, which is transmitted to the Micro-Controller Unit (MCU) for storage, calculation, and matching. The finger-vein collection device is shown in Fig. 4.
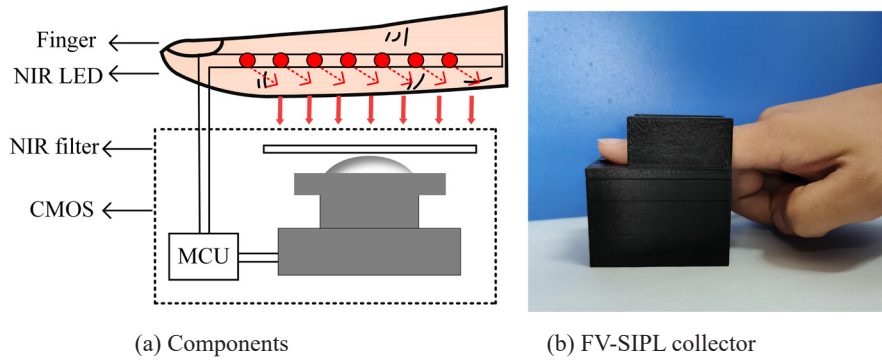

(a) Components   (b) FV-SIPL collector

Fig. 4. Our self-built acquisition equipment

Data Preprocessing. The range and resolution of finger vein images collected by different acquisition devices are inconsistent, and the samples collected contain background irrelevant to finger-vein recognition, so it will cause interference to further finger-vein recognition. To extract meaningful information in the subsequent finger-vein recognition method, we preprocess the collected images, as shown in Fig. 5.

Taking FV-USM as an example, firstly, we can obtain contour information of the finger veins through edge detection and filters, which can smooth the images, suppress the noise, and eliminate the sharp phenomenon. Secondly, we normalize the RoI obtained by cropping the boundary lines. More important, FV-SIPL collected by our team contains fewer non-finger areas, no significant flipping, and no RoI extraction needed. Examples of preprocessed images from different datasets are shown in Fig. 6.
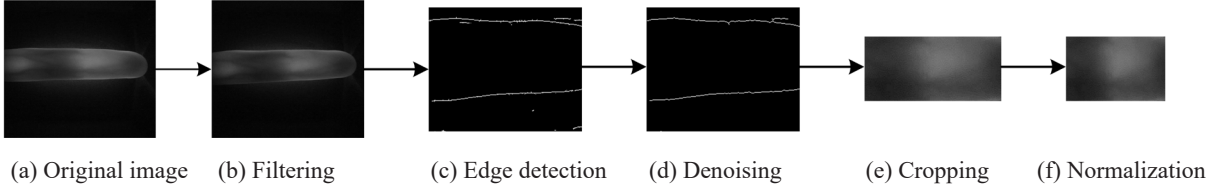
(a) Original image   (b) Filtering   (c) Edge detection   (d) Denoising   (e) Cropping   (f) Normalization

Fig. 5. Image preprocessing processes on FV-USM

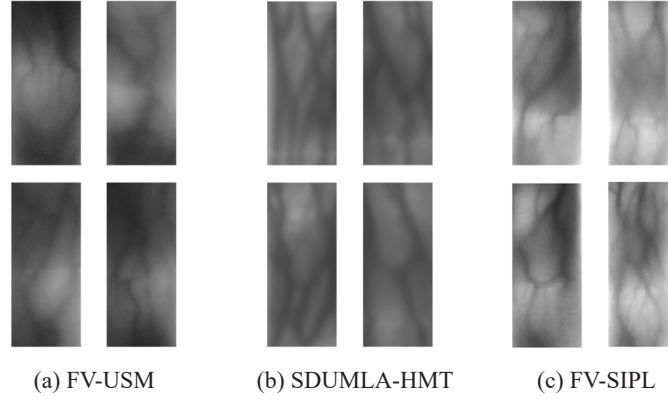(a) FV-USM   (b) SDUMLA-HMT   (c) FV-SIPL

Fig. 6. Examples of testing finger-vein datasets

4.2 Parameter Settings

We tuned the parameters on FV-USM for the proposed method in two stages: the filtering stage and the histogram calculation.

(1) Parameters in the multi-scale Log-Gabor filter: In our proposed work, we employ a multi-scale log-Gabor filter to capture more frequency information, rather than a simple log-Gabor filter or Gabor filter [33]. The parameters in the multi-scale log-Gabor filter include the minimal wavelength λ_{min}, the multiplication factor of wavelength μ, the scale number, and the ratio factor $\sigma_{ratio} = 2$. For example, with $\lambda_{min} = 4$, $\mu = 0.45$, $S = 3$, and $\sigma_{ratio} = 2$ as the initial values for FV-USM, the above parameters are tested and compared in Fig. 7. After those parameter tuning experiments, we chose $\lambda_{min} = 6$, $\mu = 0.35$, $S = 3$, and $\sigma_{ratio} = 3$.

(a) λ_{min} (b) μ
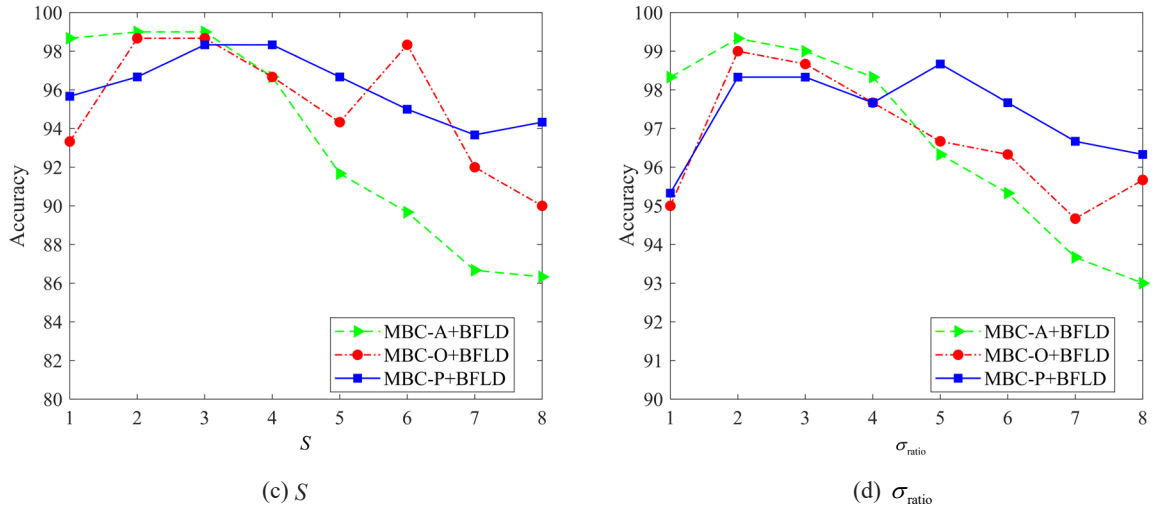
(c) S

(d) σ_{ratio}
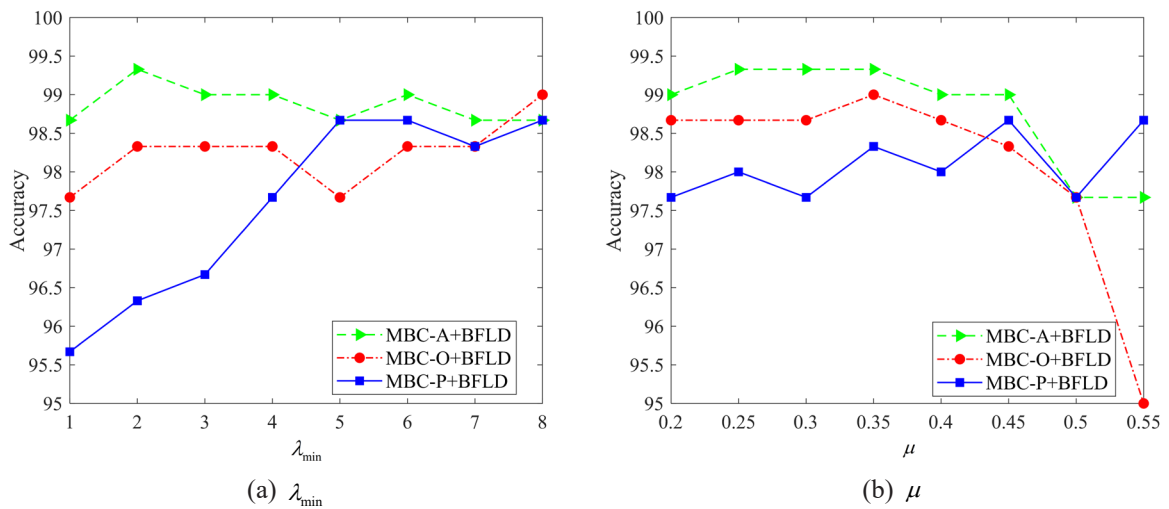
Fig. 7. The accuracy of the $MBC - X + BFLD$ combined with different parameter settings, where $X \in \{A,O,P\}$

(2) Number of blocks in the sub-region histogram: Because the block number in the sub-region determines the expressive ability and dimension of the feature, it is essential to choose an appropriate block number and further retain more detailed information. While calculating sub-region histograms, we divide the image into $M_a \times M_b$ blocks, further split into $M_c \times M_d$ sub-blocks. We have conducted ablation studies on different parent blocks and sub-block partitioning. The more blocks, the more feature dimensions, the more memory and longer recognition run-times it will cost. Under the same parameter settings, the recognition performance of FV-USM in different block division is shown in Fig. 8. Consequently, the parent block in the three datasets are divided into 1×2 sub-blocks. Finally, the sub-blocks are further separated into 1×2 for FV-USM and 2×2 for the others.
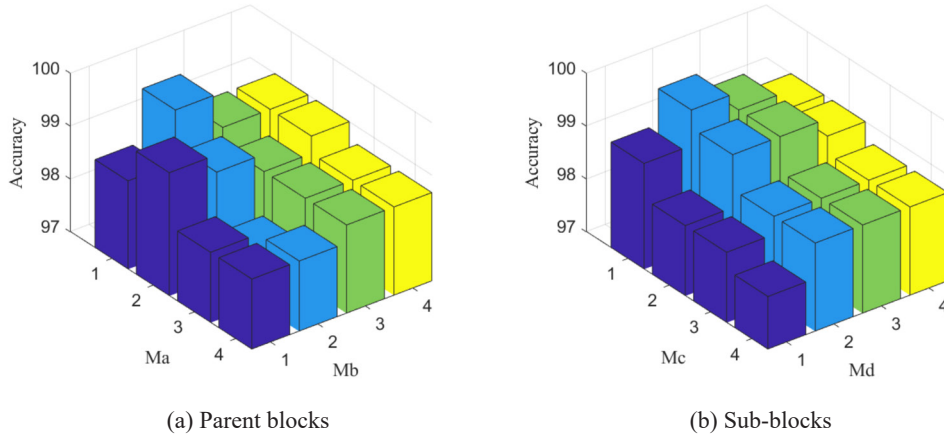

(a) Parent blocks

(b) Sub-blocks

Fig. 8. The recognition performance of FFV-MBC using different block partitions

4.3 Experimental Results

This section mainly reports the experimental results and details of FFV-MBC on two public datasets and one self-built dataset. The dataset division and selection of weight are shown. Our proposed method shows better accuracy and EER than other state-of-the-art methods.

Experiments on FV-SIPL. We used all the categories in the FV-SIPL dataset. We randomly selected four images for training, three images for verification, and three images for testing in each category in a non-repeated manner. The experimental results of FV-SIPL under different weights are shown in Table 2. All of them performed well,

especially the best weights in terms of accuracy and recognition run-time, $a_1 = 0.6$, $a_2 = a_3 = 0.2$, are chosen for later experiments. The comparison results of the FFV-MBC method with LBP, LBP+PCA, and other classical algorithms are shown in Table 3. Compared with classical algorithms such as LBP and LDA, FFV-MBC not only considers the information of the center pixel itself but also extracts more discriminative features by BFLD. Therefore, the method shows better performance in terms of accuracy and equal error rate.

Table 2. Recognition accuracy and run-time on FV-SIPL fused with different weights

a_1	a_2	a_3	Accuracy (%)	Run-time (ms)
0.2	0.4	0.4	99.38	19.78
0.4	0.3	0.3	99.38	19.81
0.6	0.2	0.2	**99.69**	**19.38**
0.8	0.1	0.1	99.69	19.77

Table 3. Comparison of run-time, accuracy, and equal error rates with different methods on the FV-SIPL dataset

Method	Run-time (ms)	Accuracy (%)	EER (%)
LBP [34]	**12.05**	83.75	6.53
LBP+PCA [35]	33.70	93.56	5.13
2DPCA [36]	73.33	97.72	3.53
LDA [37]	41.26	91.15	5.29
FFV-MBC	19.81	**99.69**	**0.85**

Experiments on FV-USM. We randomly selected 150 classes in the FV-USM dataset and generated finger vein images with the size of 100×300 pixels through the preprocessing in Fig. 5. We divided the selected images into a training set, validation set, and test set equally. Table 4 shows the experimental fusion results on the FV-USM dataset, where $a_1 = 0.2$ and $a_1 = 0.4$ have the same accuracy and similar recognition run-time. Considering the equalization of features and robustness of the algorithm, we choose the weight $a_1 = 0.4$. First, reported the accuracies in Table 5. The proposed method achieves 99.67% accuracy, better than other novel methods. Second, Table 6 shows that the FFV-MBC method has lower EER than EMC [38], lightweight CNN [39], MULBP + Block (2D)^{2}PCA [40], PLPQ [41], and FVRAS-Net [42].

Table 4. Recognition accuracy and run-time on FV-USM fused with different weights

a_1	a_2	a_3	Accuracy (%)	Run-time (ms)
0.2	0.4	0.4	99.67	11.84
0.4	0.3	0.3	**99.67**	11.67
0.6	0.2	0.2	99.33	11.14
0.8	0.1	0.1	99.33	**10.95**

Table 5. Accuracies on FV-USM compared with existing methods

Paper	Feature extraction method	Accuracy (%)
Zhao et al. [12]	CLBP+SLBP	97.43
Vasilopoulos et al. [38]	EMC	90.50
Zhao et al. [39]	lightweight CNN	97.95
Hu et al. [40]	MULBP + Block (2D)^{2}PCA	99.32
Ma et al. [41]	PLPQ	97.83
Proposed	FFV-MBC	**99.67**

Table 6. Comparison of equal error rates with different methods on the FV-USM dataset

Paper	Feature extraction method	EER (%)
Vasilopoulos et al. [38]	EMC	1.42
Zhao et al. [39]	lightweight CNN	1.07
Hu et al. [40]	MULBP + Block (2D)^{2}PCA	1.89
Ma et al. [41]	PLPQ	1.92
Yang et al. [42]	FVRAS-Net	0.95
Proposed	FFV-MBC	**0.92**

Experiments on SDUMLA-HMT. We tested FFV-MBC on 100 classes in the SDUMLA-HMT dataset. Similar to the FV-USM dataset, we also equally divided the selected data into three non-repeated parts. The fusion experiment results in Table 7 show that when $a_1 = 0.4$, $a_2 = a_3 = 0.3$, the best recognition accuracy is achieved with the shortest run-time. Compared with other advanced methods such as PLS-DA [20] and Coding Scheme B [44], the proposed method improved accuracy by 0.34% to 4.01% and reduced EER by 0.18% to 0.76%, as shown in Table 8 and Table 9.

Table 7. Recognition accuracy and run-time on SDUMLA-HMT fused with different weights

a_1	a_2	a_3	Accuracy (%)	Run-time (ms)
0.2	0.4	0.4	98.39	6.66
0.4	0.3	0.3	**98.53**	**5.97**
0.6	0.2	0.2	97.58	6.12
0.8	0.1	0.1	97.58	6.25

Table 8. Accuracies on SDUMLA-HMT compared with existing methods

Paper	Feature extraction method	Accuracy (%)
Zeng et al. [15]	CRF-RNN	90.07
Zhang et al. [20]	PLS-DA	97.52
Li et al. [43]	DSFD	94.52
Ren et al. [44]	Coding Scheme B	96.67
Zhang et al. [45]	Robust Keypoint Correspondence Clustering	97.54
Proposed	FFV-MBC	**98.53**

Table 9. Comparison of equal error rates with different methods on the SDUMLA-HMT dataset

Paper	Feature extraction method	EER (%)
Zeng et al. [15]	CRF-RNN	5.83
Zhang et al. [20]	PLS-DA	2.15
Yang et al. [42]	FVRAS-Net	1.71
Ren et al. [44]	Coding Scheme B	2.14
Liu et al. [46]	Shallow CNN	2.29
Proposed	FFV-MBC	**1.53**

4.4 Ablation Studies

In order to verify the importance of fusing the three components to improve the finger-vein recognition performance. We compared the accuracy of the FFV-MBC with the three components of MBC without and with dimension reduction shown in Table 10. Experimental results show that BFLD can further improve the performance of the MBC algorithm in terms of amplitude, direction, and phase component and improve the recognition rate by 0.39% to 3%. On this basis, we fuse the three components in a certain proportion, namely FFV-MBC. Our FFV-MBC outperforms MBC and MBC+BFLD methods to a certain degree. Especially for the FV-USM dataset with uneven illumination, the recognition performance is significantly improved after fusing the three components.

Table 10. Experimental results of the proposed algorithm under different combinations

Methods	MBC-A	MBC-O	MBC-P	MBC-A+BFLD	MBC-O+BFLD	MBC-P+BFLD	FFV-MBC
FV-SIPL (%)	98.15	96.76	98.77	99.07	98.61	99.38	**99.69**
FV-USM (%)	97.67	95.67	96.33	99.00	98.67	98.33	**99.67**
SDUMLA-HMT (%)	97.58	98.00	96.77	98.39	98.39	97.58	**98.53**

4.5 Result Analysis

The algorithm can effectively obtain meaningful information from finger vein images since the monogenic signal is represented by local amplitude, phase, and orientation. The intensity encoding process in MBC can compensate for the representation capability of local variation and improve the recognition accuracy. After that, BFLD is exploited to reduce the dimension of the encoded feature vector, which can obtain stable and effective feature

extraction and significantly improve the recognition effect, as shown in the experimental results of Table 10.

The number of blocks is also an essential factor affecting the recognition effect. Block partitions of parents and sub-blocks have been tuned to find the best accuracy. As shown in Fig. 8, the accuracy of the FFV-MBC method increases first and then decreases with the increasing number of blocks. It shows that when the number of blocks is too large, although the small local change information of the image has been accurately extracted, it may face an insufficient grasp of the larger regional feature information. The fusion experiments of the three datasets show that choosing weights can noticeably improve the recognition accuracy without increasing the run-time.

Thanks to FFV-MBC fuses three meaningful features, the method achieves higher accuracy and lower equal error rate on three datasets compared with classical methods and state-of-the-art methods, reflecting the superiority of the FFV-MBC method.

5 Conclusions

To address the problem of poor feature pattern representations in traditional finger-vein recognition algorithms, we propose a novel fused finger-vein recognition method based on monogenic binary coding. We utilize a multi-scale Log-Gabor filter to acquire three components of images, i.e., amplitude, orientation, and phase information. Also, the BFLD is used to reduce the dimensions of the extracted features, including redundant information. Finally, for each image, the similarities of amplitude, orientation, and phase information are combined under appropriate weights, calculated from cosine similarities. The experimental results verify that the combination of the monogenic signal components in the FFV-MBC can effectively represent the finger-vein features. The superiority of the proposed FFV-MBC over most classical and state-of-the-art methods on three different datasets. Besides these, the finger-vein dataset we made eliminates image preprocessing steps and results in excellent performance for finger-vein recognition. Although the extracted features in the proposed method consider the information of the relationship between the center pixel and the surrounding pixels as well as the information of the center pixel itself, these features are all local features and ignore the importance of global information. Therefore, we will consider encoding global information and fusing local and global features in future studies. Design more efficient encoding and feature representation methods to improve the accuracy and robustness of finger vein and other biometric identification methods.

6 Acknowledgement

References

[1] Z.-D. Wu, Y.-N. Wang, J.-W. Zhang, Fouling and damaged fingerprint recognition based on deep learning, Journal of Electronics and Information Technology 39(7)(2017) 1585-1591.

[2] P. Poonia, P.-K. Ajmera, V. Shende, Palmprint recognition using robust template matching, Procedia Computer Science 167(2020) 727-736.

[3] C.-K. Jing, T. Song, L. Zhang, L. Wang, K.-L. Liu, A survey of face recognition technology based on deep convolutional neural networks, Computer Applications and Software 35(1)(2018) 223-231.

[4] P.-R. Nalla, A. Kumar, Toward more accurate iris recognition using cross-spectral matching, IEEE Transactions on Image Processing 26(1)(2017) 208-221.

[5] L. Yang, G.-P. Yang, Y.-L. Yin, L.-Z. Zhou, A survey of finger vein recognition, in: Proc. Chinese conference on biometric recognition, 2014.

[6] W. Song, T. Kim, H.C. Kim, J.H. Choi, H.-J. Kong, S.-R. Lee, A finger-vein verification system using mean curvature, Pattern Recognition Letters 32(11)(2011) 1541-1547.

[7] G.-Q. Wang, J. Wang, Sift based vein recognition models: analysis and improvement, Computational and Mathematical Methods in Medicine (2017) 2373818.

[8] Y. Lu, S. Yoon, S.-J. Xie, J.-C. Yang, Z.-H. Wang, D.-S. Park, Finger Vein Recognition Using Histogram of Competitive Gabor Responses, in: Proc. 2014 22nd International Conference on Pattern Recognition, 2014.

[9] J.-D. Wu, C.-T. Liu, Finger-vein pattern identification using svm and neural network technique, Expert Systems with Applications 38(11)(2011) 14284-14289.

[10] J.-D. Wu, C.-T. Liu, Finger-vein pattern identification using principal component analysis and the neural network technique, Expert Systems with Applications 38(5)(2011) 5423-5427.

[11] S. Balakrishnama, A. Ganapathiraju, Linear discriminant analysis-a brief tutorial, Institute for Signal and information Processing 18(1998) 1-8.

[12] Y. Zhao, J.-C. Yang, Y.-J. Bao, H.-B. Song, Trustworthy authorization method for security in Industrial Internet of Things, Ad Hoc Networks 121(2021) 102607.

[13] P. Cui, X.-T. Zhang, A block-based bi-directional Fisher linear discriminant analysis on face recognition, Journal of Optoelectronics·Laser 27(4)(2016) 421-428.

[14] J. Wang, H.-J. Li, G.-Q. Wang, M. Li, D. Li, Vein recognition based on (2D) 2FPCA, International Journal of Signal Processing, Image Processing and Pattern Recognition 6(4)(2013) 323-332.

[15] J.-Y. Zeng, F. Wang, J.-X. Deng, C.-B. Qin, Y.-K. Zhai, J.-Y. Gan, V. Piuri, Finger Vein Verification Algorithm Based on Fully Convolutional Neural Network and Conditional Random Field, IEEE Access 8(2020) 65402-65419.

[16] W. Song, T. Kim, H.C. Kim, J.H. Choi, H.-J. Kong, S.-R. Lee, A finger-vein verification system using mean curvature, Pattern Recognition Letters 32(11)(2011) 1541-1547.

[17] N. Miura, A. Nagasaka, T. Miyatake, Feature extraction of finger-vein patterns based on repeated line tracking and its application to personal identification, Machine vision and applications 15(4)(2004) 194-203.

[18] J.-F. Yang, X. Zhang, Feature-level fusion of fingerprint and finger-vein for personal identification, Pattern Recognition Letters 33(5)(2012) 623-628.

[19] C. Vasilopoulos, A. Skodras, A Novel Finger Vein Recognition System Based on Enhanced Maximum Curvature Points, in: Proc. 2018 IEEE 13th Image, Video, and Multidimensional Signal Processing Workshop, 2018.

[20] L.-P. Zhang, L.-J. Sun, W.-J. Li, J.-M. Zhang, W.-W. Cai, C.-T. Cheng, X. Ning, A Joint Bayesian Framework based on Partial Least Squares Discriminant Analysis for Finger Vein Recognition, IEEE Sensors Journal 22(1)(2021) 785-794.

[21] C.-G. Liu, Y.-H. Kim, An efficient finger-vein extraction algorithm based on random forest regression with efficient local binary patterns, in: Proc. 2016 IEEE International Conference on Image Processing, 2016.

[22] B.A. Rosdi, C.W. Shing, S.A. Suandi, Finger vein recognition using local line binary pattern, Sensors, 11(12)(2011) 11357-11371.

[23] A.A. Mustafa, A.A.K. Tahir, A new finger-vein recognition system using the complete local binary pattern and the phase only correlation, International Journal of Advances in Signal and Image Sciences 7(1)(2021) 38-56.

[24] C.-C. Zhao, H.-M. Lu, Y.-P. Li, W.-Y. Liu, R.-R. Gao, A Novel Local Binary Operator Based on Discretization for Finger Vein Recognition, in: Proc. Chinese Conference on Biometric Recognition, 2021.

[25] M. Felsberg, G. Sommer, The monogenic signal, IEEE transactions on signal processing 49(12)(2012) 3136-3144.

[26] A. Kumar, N. Agrawal, I. Sharma, S. Lee, H.N. Lee, Hilbert transform design based on fractional derivatives and swarm optimization, IEEE Transactions on Cybernetics 50(5)(2018) 2311-2320.

[27] Z. He, Gesture recognition based on tri-axis accelerometer using 1d gabor filters, in: Proc. 2018 9th International Symposium on Parallel Architectures, Algorithms and Programming, 2018.

[28] A. Hajian, D.A. Ramli, Sharpness enhancement of finger-vein image based on modified un-sharp mask with log-Gabor filter, Procedia Computer Science 126(2018) 431-440.

[29] M. Yang, L. Zhang, S.C.K. Shiu, D. Zhang, Monogenic binary coding: An efficient local feature extraction approach to face recognition, IEEE Transactions on Information Forensics and Security 7(6)(2012) 1738-1751.

[30] M.S.M. Asaari, S.A. Suandi, B.A. Rosdi, Fusion of band limited phase only correlation and width centroid contour distance for finger based biometrics, Expert Systems with Applications 41(7)(2014) 3367-3382.

[31] Y. Yin, L. Liu, X. Sun, SDUMLA-HMT: A Multimodal Biometric Database, Springer Berlin Heidelberg, Springer Berlin Heidelberg 7098(2011) 260-268.

[32] R. Ramachandra, K.B. Raja, S.K. Venkatesh, C. Busch, Design and development of low-cost sensor to capture ventral and dorsal finger vein for biometric authentication, IEEE Sensors Journal 19(15)(2019) 6102-6111.

[33] M. Yang, L. Zhang, L. Zhang, D. Zhang, Monogenic binary pattern (MBP): A novel feature extraction and representation model for face recognition, in: Proc. 2010 20th international conference on pattern recognition, 2010.

[34] E.C. Lee, H.C. Lee, K.R. Park, Finger vein recognition using minutia-based alignment and local binary pattern-based feature extraction, International Journal of Imaging Systems and Technology 19(3)(2009) 179-186.

[35] Y. Luo, C.-M. Wu, Y. Zhang, Facial expression recognition based on fusion feature of PCA and LBP with SVM, Optik-International Journal for Light and Electron Optics 124(17)(2013) 2767-2770.

[36] H. Ma, Finger Vein Identification Based on 2DPCA, Advanced Materials Research 988(2014) 548-551.

[37] J.-W. Lu, K.N. Plataniotis, A.N. Venetsanopoulos, Face recognition using LDA-based algorithms, IEEE Transactions on Neural networks 14(1)(2003) 195-200.

[38] C. Vasilopoulos, A. Skodras, A Novel Finger Vein Recognition System Based on Enhanced Maximum Curvature Points, in: Proc. 2018 IEEE 13th Image, Video, and Multidimensional Signal Processing Workshop, 2018.

[39] D.-D. Zhao, H. Ma, Z.-D. Yang, J.-N. Li, W.-B. Tian, Finger vein recognition based on lightweight CNN combining center loss and dynamic regularization, Infrared Physics & Technology 105(2020) 103221.

[40] N. Hu, H. Ma, T. Zhan, Finger vein biometric verification using block multi-scale uniform local binary pattern features and block two-directional two-dimension principal component analysis, Optik 208(2020) 163664.

[41] H. Ma, N. Hu, C. Fang, The biometric recognition system based on near-infrared finger vein image, Infrared Physics & Technology 116(2021) 103734.

[42] W.-L. Yang, W. Luo, W.-X. Kang, Z.-X. Huang, Q.-X. Wu, FVRAS-Net: An Embedded Finger-Vein Recognition and

AntiSpoofing System Using a Unified CNN, IEEE Transactions on Instrumentation and Measurement 69(11)(2020) 8690-8701.

[43] S. Li, B. Zhang, An adaptive discriminant and sparsity feature descriptor for finger vein recognition, in: Proc. 2021-2021 IEEE International Conference on Acoustics, Speech and Signal Processing, 2021.

[44] H.-Y. Ren, L.-J. Sun, J. Guo, C. Han, F. Wu, Finger vein recognition system with template protection based on convolutional neural network, Knowledge-Based Systems 227(2021) 107159.

[45] G. Zhang, X.-J. Meng, High Security Finger Vein Recognition Based on Robust Keypoint Correspondence Clustering, IEEE Access 9(2021) 154058-154070.

[46] J.-Z. Liu, Z.-Y. Chen, K.-Y. Zhao, M.-J. Wang, Z. Hu, X.-W. Wei, Y.-C. Zhu, Y.-C. Yu, Z. Feng, H. Kim, C.-L. Jin, Finger Vein Recognition Using a Shallow Convolutional Neural Network, in: Proc. Chinese Conference on Biometric Recognition, 2021.